Incoherent Imaging at Microwave and Millimeter-Wave Frequencies Using Noise Transmitters

Jeffrey A. Nanzer, Stavros Vakalis, Liang Gong, Yuxiao He, and John Papapolymerou

Electrical and Computer Engineering Department, Michigan State University, 428 South Shaw Lane 2120 Engineering Building, East Lansing, MI 48824.

Correspondence to: nanzer@msu.edu

Introduction

Imaging represents one of the most significant and widely used methods of conveying information in scientific settings and society more broadly, due to the inherent human ability to quickly process spatial information. Traditionally an optical technique, an increasing number of applications, such as aerial imaging through clouds and fog [1], medical and through-the wall imaging [2, 3], and contraband detection [4, 5], require imaging through materials that are opaque to optical and infrared wavelengths. The microwave (3-30 GHz) and millimeter-wave (30-300 GHz) bands electromagnetic spectrum are particularly well suited to these applications due to their ability to propagate through materials, obscurants, and even some building wall materials with minimal attenuation [5]. Many approaches are based on passive sensing of thermally-generated signals, which can be implemented with sparse array apertures in a staring configuration that does not require electrical or mechanical scanning; however, thermal radiation at microwave and millimeter-wave frequencies is extremely low in power, necessitating costly highsensitivity hardware [5, 6]. Active imaging systems can achieve increased sensitivity by illuminating the scene and capturing the scattered signals. However, such systems typically require some form of scanning by either physically moving the aperture, which can lead to long data acquisition time, or electrical scanning using phased antenna arrays, which can require a large number of active components. In this article we review a recently developed imaging technique that combines beneficial aspects of both passive and active imaging approaches call active incoherent millimeter-wave (AIM) imaging. This technique illuminates the scene with noise signals mimicking the properties of thermal radiation, enabling the use of a sparse receiving array and imaging in a staring format, without scanning. Because the scene is actively illuminated, significantly higher received signal power is captured than in passive systems, thereby enabling the use of low-cost hardware.

Initially, methods for generating radio-frequency (RF) images focused on mechanically-scanned systems that used large reflector antennas on motorized gimbals. In such systems the imaging process can be lengthy, the size is often too large for reasonable portability, and the power requirements of the motors tend to be large. Holographic imaging systems have the drawback of long data acquisition times [7]. Synthetic Aperture Radar (SAR) has long been used for remote imagery of the ground or individual objects [8], however, the necessity of scanning an individual platform or antenna over a long baseline to synthesize a larger aperture inherently negates the ability to form images rapidly, and images can be corrupted by moving objects or changing scenes. Phased antenna arrays provide a number of benefits over mechanically-scanned systems due to their inherent flexibility and the fact that they can be implemented in planar form, easing size and weight concerns [9]. And although electronic beam steering can be accomplished more quickly than mechanical steering, it is challenging and costly to develop millimeter-wave phased arrays achieving fine angular resolution due to the large number of elements involved, the small element spacing, and heat dissipation requirements.

Coherent computational imaging approaches provide one answer to the need for staring millimeter-wave imaging. By leveraging coded apertures that illuminate the scene with a pseudo-random radiation pattern, staring image reconstruction with shorter data acquisition time and fewer antenna elements than traditional phased arrays has been demonstrated [10, 11]. The common shortcomings of computational microwave imaging are the long image reconstruction times due to the heavy computational loads and the need for precise

knowledge of the transmit illumination at every point in space and every instance in time. A less common staring imaging approach that inspired our work is passive interferometric millimeter-wave imaging [12, 13]. First developed in radio astronomy [14], interferometric imaging uses sparse antenna arrays to capture thermally generated electromagnetic radiation of astronomical sources. More recently the technique has been used in security sensing by capturing thermal radiation [6]. Interferometric antenna arrays are sparse compared to traditional phased arrays, leading to lower hardware implementation concerns, and interferometric image reconstruction algorithms are based on fast Fourier transforms which generally have low computational complexity. Additionally, there is no one-to-one correspondence between pixels and antennas, which is the case in focal plane arrays that are a more common starting-type imager. In interferometric imaging, each element is simultaneously capturing information associated with the entire image, which makes the system tolerant to element failures. Nonetheless, because passive millimeter-wave imaging systems capture the thermally generated electromagnetic radiation, which is on the order of femtowatts [5], they require very highly sensitive receivers. The sensitivity ΔT of a radiometric receiver measuring thermal radiation is inversely proportional to the square root of system bandwidth B and integration time τ by $\Delta T \propto \frac{1}{\sqrt{B\tau}}$ [5,15]. Passive systems thus necessitate receivers with high bandwidths and long integration times, as well as amplifiers with gain on the order of 100 dB or greater, leading to high system cost. However, since the radiation is noise-like, passive imagers can leverage the Van Cittert-Zernike theorem [14, 16], which indicates that noise-like signals that are spatially and temporally incoherent and are captured by interferometric apertures can be used to reconstruct images of the scene, provided that a sufficient number of interferometric baselines are utilized. The spatio-temporal incoherence requirement means that each point in space should act like an independent noise-like radiator as a function of time. These systems capture information in the spatial frequency domain, and through inverse Fourier transform (IFT), reconstruct the spatial image. The result is that passive systems can be implemented with significantly fewer array elements than active imagers, often an order of magnitude less. But since this approach requires spatial and temporal incoherence, active illumination from coherent sources, as are typically used in active imaging systems, is not compatible.

AIM imaging is a new form of computational millimeter-wave imaging that retains the benefits of interferometric imaging without the need for highlysensitive and overly expensive receivers with wide bandwidth and long integration time. This is achieved by actively illuminating the scene using multiple noise transmitters and mimicking the properties of thermal radiation, yielding a much higher signal-to-noise ratio (SNR) than passive systems. As a result, both integration time and bandwidth are at least an order of magnitude smaller than passive millimeter-wave imaging [17]. With this method, scanning through physical or electronic means, as in SAR and raster scanning techniques, is not required. Because AIM imaging samples information in the spatial frequency domain, the technique operates in snapshot mode, meaning that no beamscanning is required, as is the case with phased arrays. Furthermore, interferometric arrays use significantly less antenna elements and hardware than phased arrays which leads to significantly lower system cost [18]. Compared to computational imaging techniques which typically solve an inverse problem and require accurate knowledge of the illumination, AIM imaging is based on matrix multiplications and fast Fourier processing which are significantly faster than matrix inversions and iterative algorithms. Additionally, this approach is different than coherent noise radar [19] because no synchronization is needed between transmitters and receivers. Unlike coherent computational imaging, no exact knowledge of the transmit radiation is required, as long as it satisfies the requirement of spatial and temporal incoherence. This leads to additional freedom in system design and makes possible the use of commercial hardware without accurate calibration. In the following, we review AIM imaging theory and present two proof-of-concept imaging systems, a synthesized array at 5.85 GHz and a static twodimensional sparse array at 40 GHz. We present experimental results of reflecting targets generated from received waveforms of 10 us, demonstrating the ability to form images quickly.

Interferometric Fourier Imaging

Spatial frequency sampling was developed in radio astronomy to synthesize large antenna apertures using a small number of physical elements [14, 20]. The concept is based on the fact that any two-dimensional image can be decomposed into a summation of signals corresponding to different spatial frequencies (Fig. 1), in the same way that a voltage waveform in the time domain can be represented by a summation of sinusoidal signals

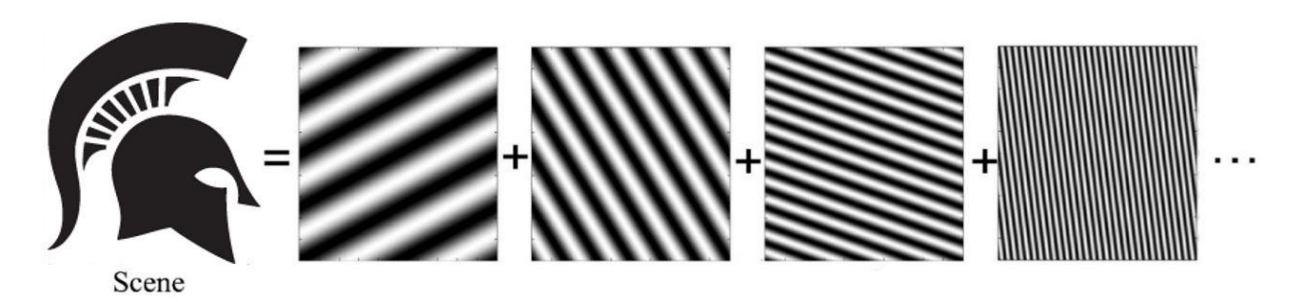


Fig. 2. A two-dimensional image can be decomposed into a summation of spatially varying signals, each corresponding to a different spatial frequency [21].

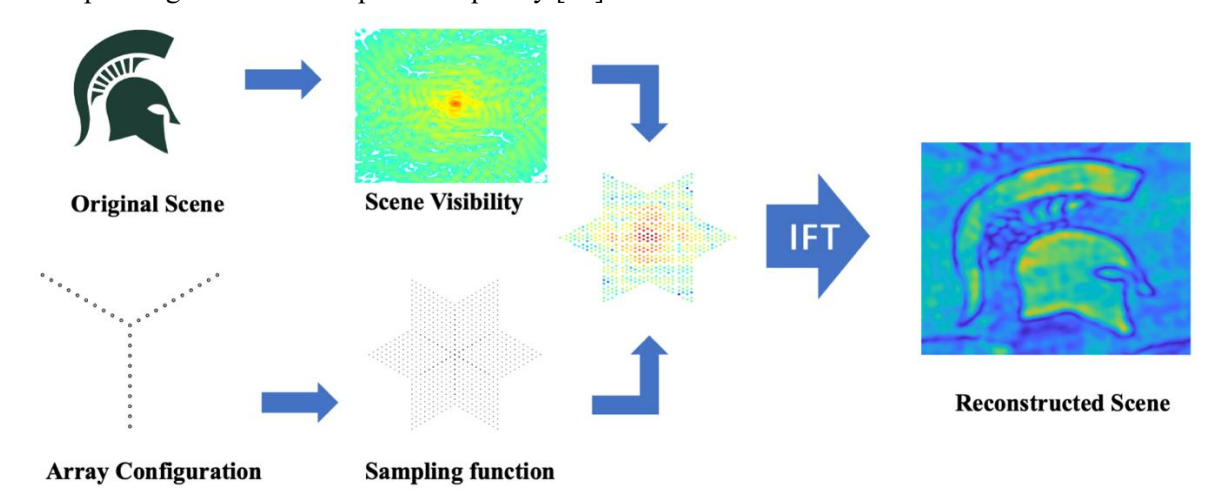


Fig. 1. Interferometric image reconstruction overview. The image is reconstructed by taking the IFT of the sampled scene visibility V(u,v), the latter being the scene information in the spatial-frequency domain. The sampled visibility is the product of the scene visibility and the sampling function, which is the set of spatial frequencies measured by the array [18].

of different frequencies. Each spatial frequency is defined in terms of a number of cycles per radian and a direction which can be measured by a pair of antennas separated by a large number of wavelengths. The outputs of each antenna pair are cross-correlated, yielding a sample of the *visibility*, the basic quantity measured by interferometric imaging systems. The image visibility is related to the image via a Fourier transform, which follows from the Van Cittert-Zernike theorem [14, 16]. The theorem states that if the radiation emanating from the scene is spatiotemporally incoherent and enough spatial frequencies are measured such that the visibility is adequately sampled, the image can be reconstructed through an IFT.

The image formation process is described in Fig. 2. The spatial sampling function of a given antenna array configuration is determined by the baselines, given by the antenna separations, in the array, and is a function of the two spatial frequency dimensions u, v which are measured in cycles per radian. Wide antenna baselines map to high spatial frequencies (those towards the edges of the

sampling function) and narrow baselines map to low spatial frequencies (towards the center of the sampling function); individual antenna responses represent a spatial frequency of zero cycles per radian, or a dc response. The scene to be imaged can be viewed in terms of its spatial frequency content by calculating its two-dimensional Fourier transform, which is its visibility V(u,v). Lower spatial frequencies in the visibility generally correspond to intensities and widely distributed information in the image, whereas high spatial frequencies capture information such as edges and other sharp features in the image. The information captured by the interferometric array is the product of the scene visibility and the sampling function, called the sampled visibility, which is then processed through an IFT to generate a reconstructed image of the scene.

The information represented in the sampled visibility directly impacts the quality of the reconstructed image. In applications where shape recognition is important, it is desirable to capture a large number of high

spatial frequency samples, which represent the edge information provided by wide antenna baselines. If intensities are of greater interest, low spatial frequencies are needed provided by narrow antenna baselines [22]. The receiving array can thus be designed appropriately to capture the desired level of information while minimizing the number of elements used in the array [23].

Interferometry Combined with Noise Radar

Implicit in the image formation process above is the assumption that the signal emanating from the scene is temporally and spatially incoherent; the Van Cittert-Zernike theorem is valid only in this case. While spatial frequency sampling has been investigated for applications such as security imaging [6, 12, 24, 25], these systems are passive and collect thermally-generated radiation from the scene. Such radiation is driven by random thermallyinduced fluctuations in materials and is inherently spatiotemporally incoherent, making Fourier-domain imaging possible. However, at millimeter-wave frequencies, this radiation is extremely low in power, often on the order of femtowatts, necessitating the use of extremely high gain receivers with wide bandwidths and long integration times to achieve the necessary sensitivity to form a reasonable image. Such constraints limit the utility of these systems to generate images quickly with low system cost.

To overcome this sensitivity limitation, we have techniques [26] combined noise radar interferometric imaging in the AIM approach. By transmitting a signal, the system sensitivity can be much lower than a passive system's, alleviating the need for high-gain and wideband receivers. However, the radiation scattered off the scene must still conform to the requirements of spatio-temporal incoherence such that the Van Cittert-Zernike theorem is still valid. Thus, for an active spatial frequency sampling system, it is necessary to transmit a signal that is temporally incoherent within the sampling interval and that is spatially incoherent within the resolution of the receiving array. To ensure that the required spatio-temporal incoherence is satisfied, we actively transmit noise signals towards the scene of interest. With multiple noise transmitters separated by a baseline equal to or larger than the receiving array, sufficient spatio-temporal incoherence can be imparted on the reflected radiation to enable Fourier image reconstruction.

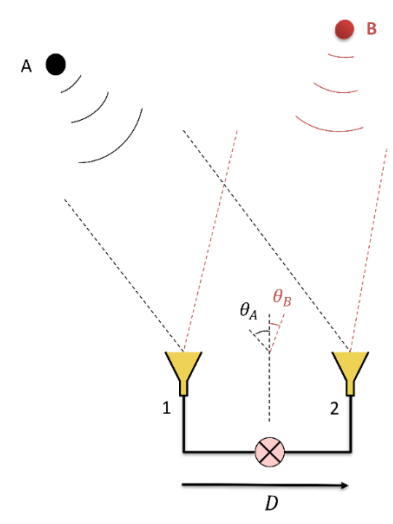


Fig. 3. Two elements of an interferometric array, forming a correlation interferometer, observing two radiating sources [18].

A given antenna pair in the interferometric receiving array collects and cross-correlates the signals scattered off the scene. For an antenna pair observing two point sources as shown in **Fig. 3**, the voltage outputs on the two receivers can be given by

$$V_1 = s_{1A} + s_{1B} + n_1$$

 $V_2 = s_{2A} + s_{2B} + n_2$

where s_{iA} and s_{iB} are the responses of the *i*th element due to the point sources A and B, respectively, and n_i is the uncorrelated noise received by the *i*th element. The output voltage of the correlation interferometer can be written as

$$V_{out} = \langle V_1 V_2 \rangle = \langle s_{1A} s_{2A} \rangle + \langle s_{1B} s_{2B} \rangle + \langle s_{1A} s_{2B} \rangle + \langle s_{1B} s_{2A} \rangle$$

where the angled brackets $\langle \cdot \rangle$ indicate time-averaging, $\langle s_{1A}s_{2A} \rangle$ and $\langle s_{1B}s_{2B} \rangle$ represent the common parts from the two point sources, and $\langle s_{1A}s_{2B} \rangle$, $\langle s_{1B}s_{2A} \rangle$ represent cross-product terms that have no actual image information and act as artifacts to the spatial frequency samples that the interferometric array collects. Using a traditional coherent transmission from a single antenna to illuminate the two point sources will result in considerable correlation between their responses, and as a result the cross-product terms will be comparable with the self-terms, which represent the actual information, causing the interferometric image reconstruction to be unsuccessful. However, using the radiation from independent multiple noise transmitters superimposing in

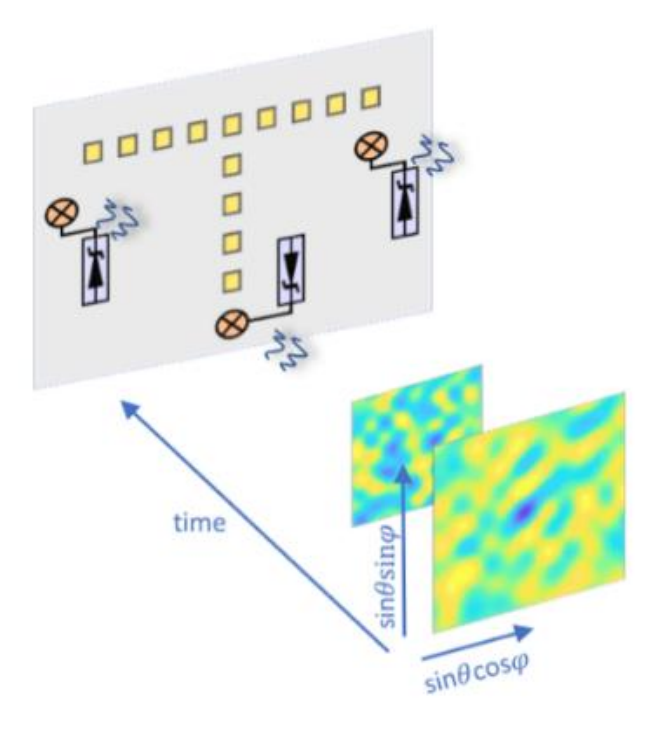


Fig. 4. Interferometric T-shaped receive array (rectangular patches), combined with three noise transmitters (represented by the circles with crosses transmitting a random signal, and the Zener diodes represent the actual noise generating circuit). The two frames travelling in space, along the time axis, represent the spatio-temporal random field transmitted from the noise transmitters, and is product of their random superposition in space. Yellow color represents high intensity, while blue represent low intensity. The horizontal and vertical axes represent the directional cosines for the azimuth and elevation planes.

the spatial domain, can make the two point responses sufficiently independent with each other. As a result, the cross-product terms will be much smaller than the selfterms, and the output voltage of the correlation interferometer can be approximated as

$$V_{out} = \langle V_1 V_2 \rangle \approx \langle s_{1A} s_{2A} \rangle + \langle s_{1B} s_{2B} \rangle.$$

The AIM concept with noise illumination can be seen in **Fig. 4**. A sparse receive array is combined with a small set of noise transmitters placed at baselines equal to or greater than the maximum baseline in the receiving array. The three noise signals are temporally incoherent, thus their superposition at a given point in space will be diverse from adjacent points in space. **Fig. 4** shows the signal intensity at various points in time (or range, equivalently) where three noise signals constructively and

destructively interfere in the azimuth and elevation planes, resulting in a radiation field incident on the scene that is both temporally and spatially incoherent. The receiving array can then process the scattered radiation by pair-wise cross-correlations, with the uncorrelated cross terms minimized, leaving the terms associated with the scene visibility. We note that the superposition of multiple communications signals can also produce a sufficiently incoherent radiation field to support the image reconstruction process [27].

Simulated AIM Imaging Process in One Dimension

We illustrate the AIM imaging approach through a simple one-dimensional simulation in this section. We model the imaging performance of a simple onedimensional scene using a non-uniform linear array of 30 elements, each element both transmitting noise and receiving the backscattered signals from the scene. The image reconstruction is a function of the azimuth angle θ in the same plane in which the linear array resides. Broadside to the array corresponds to $\theta=0$ rad, while endfire corresponds to $\theta = \pm \frac{\pi}{2}$ rad. The spacing between adjacent elements was randomized to be up to 30 wavelengths. The array in this example consists of 30 elements spaced over a total of about 125 wavelengths. Compared to a typical array on a half-wavelength grid, this array represents an 88% reduction in necessary antenna elements to achieve the same spatial resolution. Fig. 5 (a) shows the element locations. In Fig. 5 (b) the radiation pattern is shown over space and a time duration of 1 µs with the signals varying at a period of 10 ns. The broadening of the signal near the edges of the radiation pattern is due to the decreasing projected baseline at wide angles. The resulting spatio-temporal radiation is evidently random in nature, however to better assess the coherence of the radiated field, the two-dimensional autocorrelation was calculated across time and angle, shown in Fig. 5 (c). A radiation field that is perfectly spatio-temporally incoherent would result in a 2D autocorrelation response that consists of a delta function at the center; the resulting response has a strong peak at the center, and is low otherwise, indicating a strong spatio-temporal incoherence. It is important that the field be spatially incoherent between resolution bins, and temporally incoherent between time bins for the Fourier imaging process to produce reliable images.

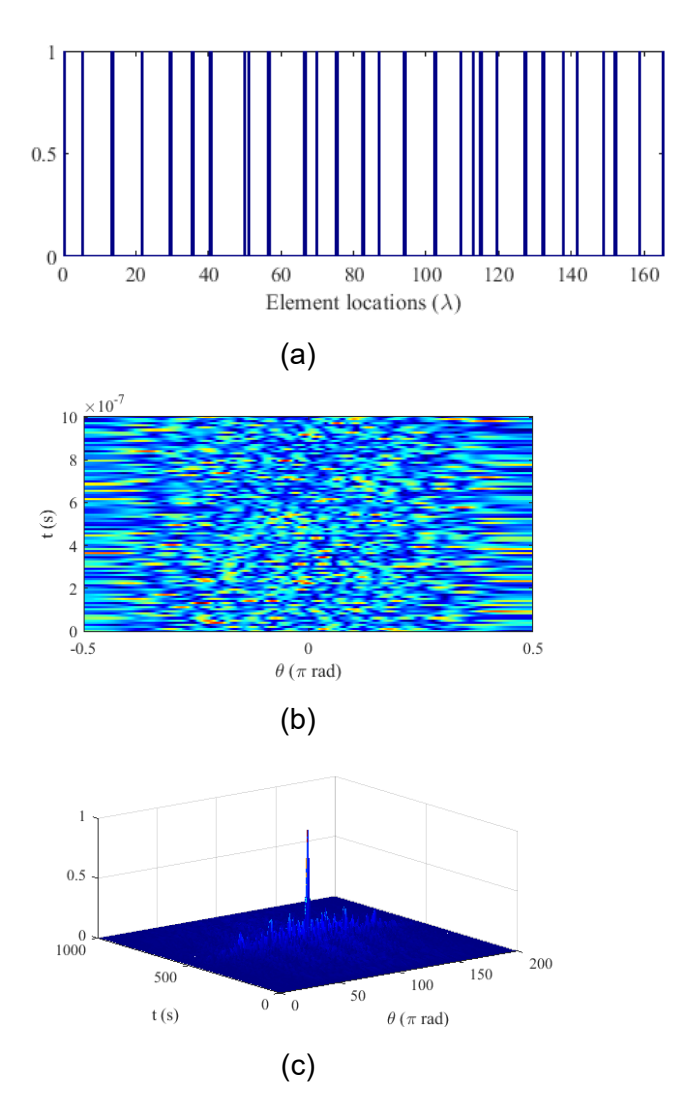


Fig. 5. (a) Randomly placed 30-element array. (b) Spatiotemporal transmit pattern with random noise generators at each element. (c) Two-dimensional autocorrelation of the transmit pattern demonstrating good spatial and temporal incoherence.

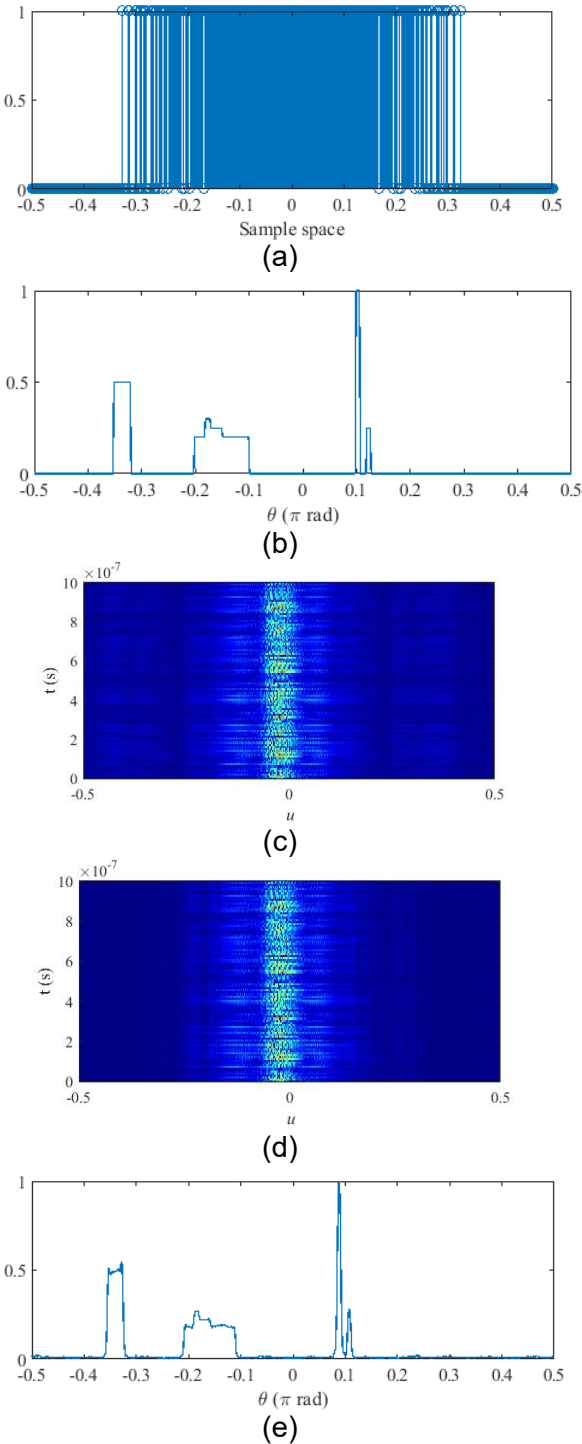
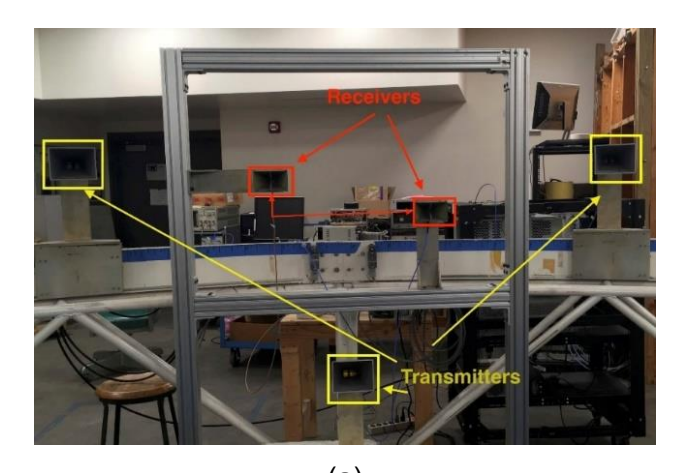


Fig. 6. (a) Sampling function of the random array. (b) Example scene to be imaged. (c) Spatio-temporal visibility of the example scene. (d) Sampled visibility (product of the sampling function and the scene visibility), which despite sampling is very close to the real visibility. (e) Reconstructed image from the 30-element random array, with a root-mean-square error of 3.4% from the original image

The antenna locations define a spatial frequency sampling function given by the different antenna separations. The sampling function for the 1D array is shown in Fig. 6 (a). An example one-dimensional scene is shown in Fig. 6 (b), and its corresponding visibility over normalized spatial frequency space (u) and time is shown in Fig. 6 (c); it can be seen that the majority of the information is contained at low spatial frequencies (where $u \sim 0$), however the higher spatial frequencies contain the information needed for spatial resolution. The sampled visibility is the product of the scene visibility and the sampling function, which is shown in Fig. 6 (d). Almost all of the low spatial frequency content has been retained; while the high spatial frequency content is reduced, there is less information at these frequencies, indicated by the lower amplitude, and thus does not contribute as much to the image reconstruction. It is clear that appropriate design of the sampling function is critical to successfully reconstruct images and capture a large amount of the image spatial frequency information. Fig. 6 (e) shows the reconstructed image which is integrated over the length of the time duration. The scene reconstruction matches well with the original scene with only 3.4% root-mean-square error, despite the fact that the element locations were chosen randomly and the array contained only 12% of the elements of a filled aperture.

5.85-GHz Experimental AIM Measurements

Experimental validation of the AIM imaging approach was conducted at two frequency bands to demonstrate the feasibility of imaging simple scenes. The first system was a two-dimensional experimental imaging system using three transmitters emitting noise signals centered at 5.85 GHz, and two receivers were sequentially moved to synthesize an inverse T-array. The transmitter locations were not moved, while the receive antennas were sequentially moved to the locations in an inverted Tarray. Because AIM imaging works by cross-correlating the collected signals pair-wise, it is possible to synthesize a larger array by sequentially collecting signals in pairs and moving the elements to cover all baselines desired in the full array. The 5.85 GHz experimental configuration that can be seen in Fig. 7 (a). The block diagram can of the experimental configuration can be seen in Fig. 7 (b).



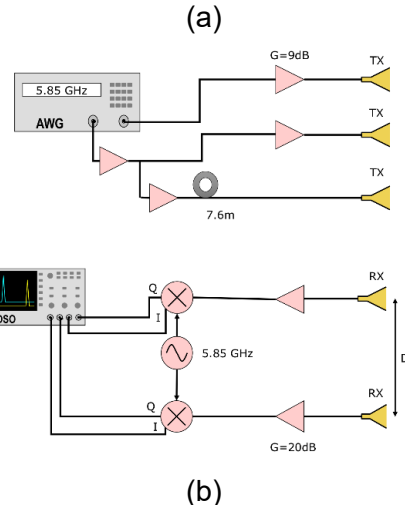


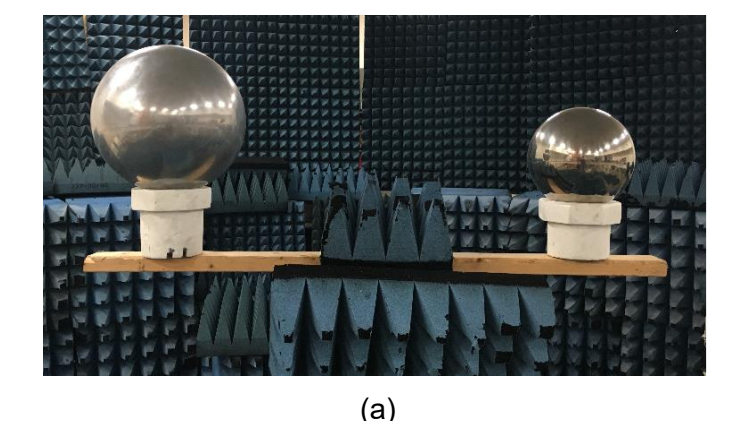
Fig. 7. (a) Experimental configuration for the 5.85 GHz experimental measurements, (b) block diagram of the experimental imaging system [17].

The noise signals were generated using a Keysight M8190 Arbitrary Waveform Generator. The noise was generated at a carrier frequency of 5.85 GHz with approximately 1 GHz of bandwidth to achieve a flat frequency response at a receive bandwidth of 25 MHz. and because only two independent outputs are available on the M8190, one of the outputs was split into two using a wideband splitter to generate two noise signals. One output of the splitter was connected to one transmitter, while the other output was connected to the second transmitter through a 7.6 m cable. This additional delay ensured that the transmitted signals were temporally uncorrelated when the signals were incident on the scene. An additional 9 dB gain amplifier with a 1 dB compression point of 19 dBm was used to overcome the losses from the splitter and the 7.6 m cable. The three transmit noise signals had a maximum power of 0 dBm

and were connected to 20 dBi standard-gain horn antennas.

The receiver consisted of two wideband horn antennas with approximately 10 dBi gain at 5.85 GHz. The synthesized array was an inverse T-array with 39 total element locations, synthesized by moving the two receiving antennas on a metal rack; no redundant baselines were collected. By moving one in the horizontal and the other in the vertical direction, the T-array was synthesized with a maximum spacing of 15\(\lambda\) in the horizontal axis and 8λ in the vertical axis, in 0.5λ increments. The narrow baselines of less than 2λ were omitted due to the physical dimensions of the horn antennas that were used. The two received signals were amplified with 20 dB low-noise amplifiers (LNAs) and downconverted to baseband using quadrature mixers with a 5.85 GHz local oscillator (LO). The four signals (I and O for each of the two antennas) were then captured using a 20 GHz Keysight MSOX92004A oscilloscope in highresolution mode. The collected signals were processed offline in MATLAB. The received signals were first lowpass filtered to a bandwidth of 25 MHz, the DC bias was removed by subtracting the average, and cross-correlation was applied to each antenna pair. The total integration time was 10 us. The utilized bandwidth and integration time are both significantly lower than those typically required in passive interferometric imaging, where bandwidths up to multiple GHz and integration times beyond 1 s are not uncommon [17]. Thus, the use of active transmission enables faster imaging with far less costly hardware than passive systems.

Experimental image reconstruction of two metal spheres, one 18 cm in radius and one 12 cm in radius, is shown in **Fig. 8** (a). The two spheres were spaced 60 cm apart on a pedestal in a 7.6 m semi-anechoic arch range, with microwave absorber placed behind the spheres. Their azimuth angle was ± 0.05 rad. The semi-anechoic arch range was smaller than the Rayleigh distance of the receiving aperture, and the targets were not located in the far-field, however, because they are located near broadside the phase errors are minimal compare to the far-field approximation [6, 28]. **Fig. 8** (b) shows the reconstructed spheres, after applying Gaussian smoothing on the reconstructed image. The left response clearly indicates the larger sphere and the lower-intensity response on the right indicates the smaller sphere.



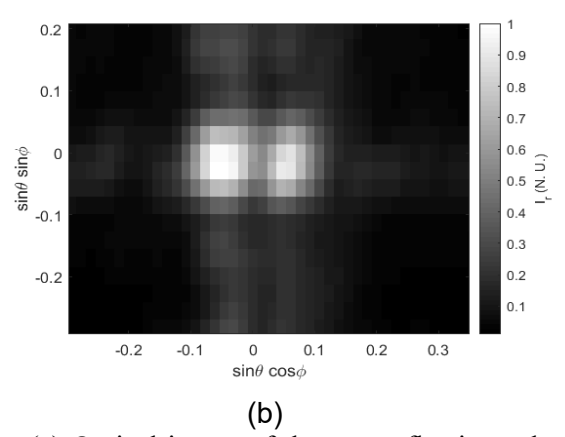


Fig. 8. (a) Optical image of the two reflecting spheres, (b) 5.85 GHz image reconstruction of the two spheres [17].

40 GHz Experimental AIM Measurements

Image resolution is dependent on the electrical size of the receiving array. While the 5.85 GHz images demonstrate the feasibility of the AIM approach, achieving better resolution necessitates an electrically larger aperture. We implemented the technique at millimeter-wave in two different systems. The first approach synthesized the receiving array in the same manner as the 5.85 GHz system by sequentially moving two receive antennas to the locations desired in a larger array. In the second approach we built a 16-element twodimensional array that captures the signals simultaneously.

For an initial investigation at millimeter-wave frequencies, two spherical targets were used as the two-dimensional scene, in the same fashion as the previous section. The schematic of the experimental configuration can be seen in **Fig. 9**. The transmitters were three 0.2-2000 MHz low-cost baseband noise sources. For a flatter

frequency response, a high pass filter with a cutoff frequency of 20 MHz was applied to each noise source before being amplified by a low-cost baseband amplifier of 30 dB gain and subsequently fed to the IF port of each upconverter. Three GaAs MMIC I/Q upconverters (Analog Devices HMC6787ALC5A), integrated with a frequency doubler for the LO and a conversion gain of 10 dB, were used to mix the noise response from baseband to 40 GHz using an LO of 20 GHz. The 40 GHz noise signals were then boosted by three 40 GHz power amplifiers, achieving approximately -10 dBm of noise power at 40 GHz with a bandwidth of approximately 1 GHz. Each transmitter was connected to a 10 dBi Ka-band horn antenna.

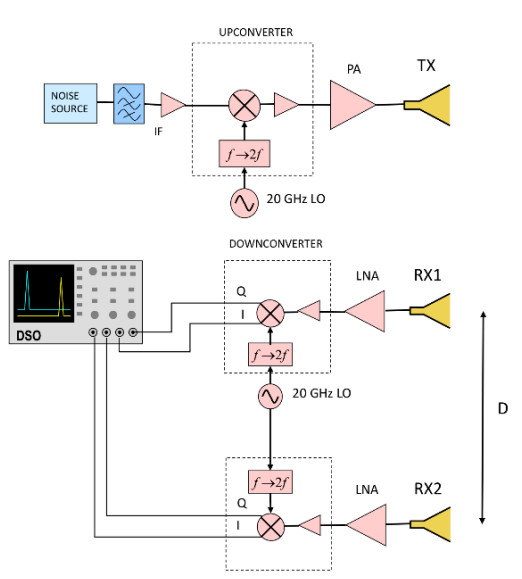
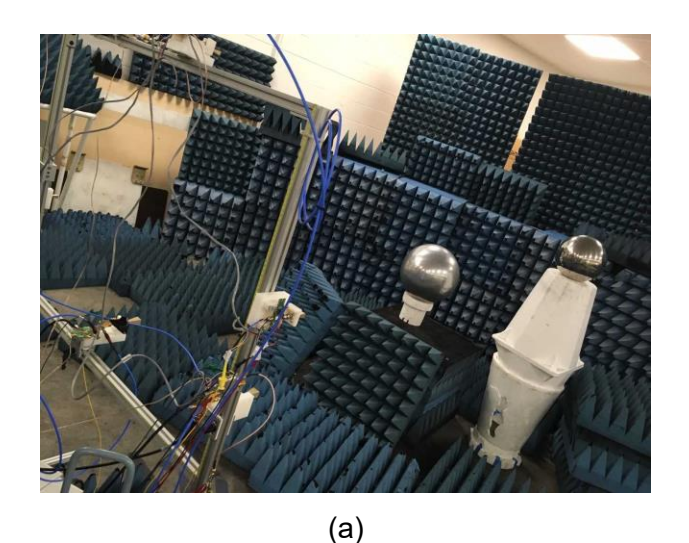


Fig. 9. The schematic of the experimental configuration for the synthesized millimeter-wave measurements. The transmitters consist of three noise sources upconverted to 40 GHz (only one shown in the figure), while the receivers consist of two elements which downconvert the received noise signal to baseband and captured using an oscilloscope [29].

For the receivers, the reflected noise was received by two 15 dBi horn antennas and amplified with 23 dB gain LNAs before downconverted to baseband using 37-44 GHz GaAs MMIC I/Q downconverters with a 3.5 dB noise figure. All the components were fixed into an aluminium rack with 3-D printed holding structures. The downconverted baseband signals were captured and

digitized using the 20 GHz Keysight MSOX92004A oscilloscope in high-resolution mode and processed offline in MATLAB. The receivers were sequentially moved to form an inverse T-array that had a maximum horizontal and vertical dimension of 66λ and 46λ , respectively.



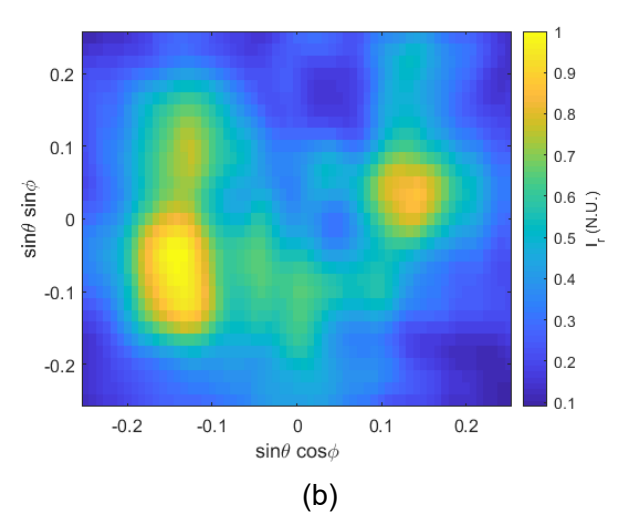
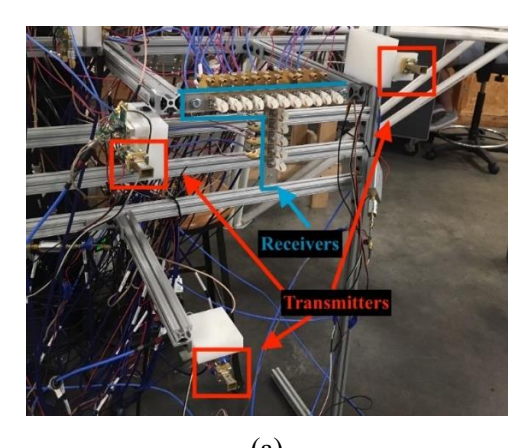


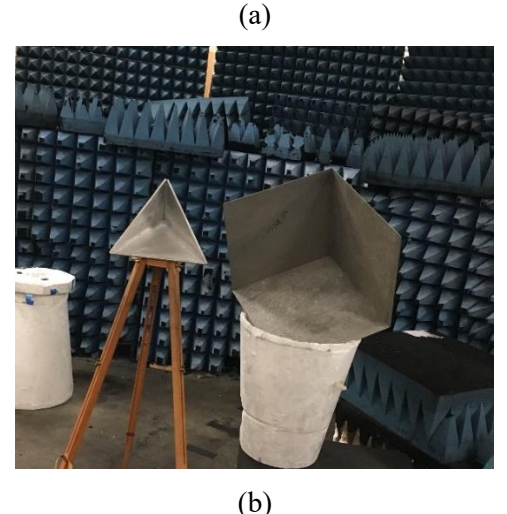
Fig. 10. (a) The two reflective spherical targets placed in the semi-closed anechoic chamber used for the synthesized millimeter-wave measurements. (b) Experimental image reconstructed intensity from the two reflective spherical targets [29].

The experimental configuration with the two reflective spheres (a) and the reconstructed image (b) can be seen in **Fig. 10**. A Gaussian filter was applied to smooth the image. The resulting image clearly shows improved resolution compared to the 5.85 GHz system,

and accurately reconstructs the relative intensities and positions of the two targets.

After the synthesized 40 GHz imaging experiments, we constructed a 16-element, 37 GHz Tshaped array to form images with a static twodimensional array. The array is shown in Fig. 11 (a), with the same three noise transmitters used in the synthesized 40 GHz imaging system. In this case, the reflected noise signals were collected by an array of 16 antipodal Vivaldi antennas that were fabricated in-house. The collected signals were amplified using the same type of LNAs and downconverters as in the synthesized 40 GHz array. The 32 quadrature responses (16 channels I and Q) were captured using two Alazartech ATS9416 16-channel, 100 MS/s waveform digitizers connected to the PCIe slots of a desktop computer. The signal processing again took place in MATLAB. We tested the static array using two corner reflectors as shown in Fig. 11 (b). The reconstructed image was processed by deconvolving the image with the calculated point-spread function (PSF) of the array, which is the impulse response in the spatial domain [30, 31]. The PSF is sometimes called the synthesized beam in interferometric imaging, and can be calculated from the 2D IFT of the sampling function. Deconvolving the image has the effect of reducing artifacts generated by the sidelobes of the PSF, typically resulting in a cleaner image. However, because traditional deconvolution can easily lead to an ill-posed problem, we used iterative blind deconvolution with the calculated PSF as an initial estimate [32]. This approach is common in aerial imaging or when using commercial hardware which are not accurately calibrated. The resulting image clearly shows the responses of the two corner reflectors with the correct locations and relative intensities.





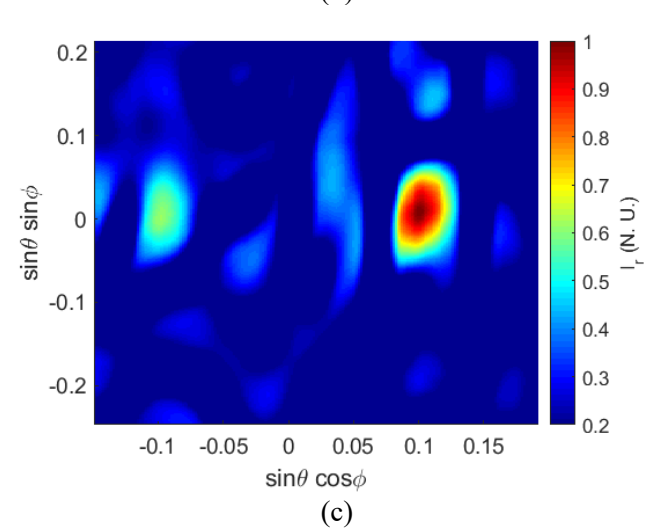


Fig. 11. (a) Photograph of the static 37 GHz AIM system with three noise transmitters and a 16-element receiver. Each receiving element consisted of an antipodal Vivaldi antenna, LNA, and quadrature downconverter. (b) The two reflective spherical targets placed in the semi-closed anechoic chamber used for the synthesized millimeterwave measurements. (c) Experimental image reconstructed intensity from the two reflective targets.

Conclusion

The demand for high-resolution millimeter-wave imaging will necessitate technologies that can provide images quickly and with minimal hardware cost. The AIM imaging technique provides one approach to achieve high-resolution imaging by combining noise radar techniques and spatial-frequency domain sampling used passive millimeter-wave imaging systems. Experimental results show the feasibility of AIM imaging using sparse antenna arrays and commercial hardware with no exact knowledge of the transmit radiation. Furthermore, the presented approach is inherently scalable, since receiver channels can potentially be developed individually and added to receiving arrays to improve resolution or increase the received signal strength. One challenge with AIM imaging is the fact that signals are not coherently processed relative to the transmitted signals, and thus additional processing gain in the form of matched filtering or pulse compression is not available, which will limit the operational range compared to traditional radar systems. Nonetheless, the received signal power is still orders of magnitude greater than that obtained in passive imaging systems, and there are numerous applications where SNR will not be the limiting factor, such as contraband detection where the environment is well controlled.

References:

- [1] H. Hellsten and L. M. H. Ulander, "Airborne array aperture UWB UHF radar-motivation and system considerations," *IEEE Aerospace and Electronic Systems Magazine*, vol. 15, no. 5, pp. 35-45, May 2000.
- [2] N. K. Nikolova, "Microwave Imaging for Breast Cancer," *IEEE Microwave Magazine*, vol. 12, no. 7, pp. 78-94, 2011.
- [3] F. Ahmad, M. G. Amin, and S. A. Kassam, "Synthetic aperture beamformer for imaging through a dielectric wall," *IEEE Transactions on Aerospace and Electronic Systems*, vol. 41, no. 1, pp. 271-283, 2005.
- [4] J. A. Nanzer, "A Review of Microwave Wireless Techniques for Human Presence Detection and Classification," *IEEE Transactions on Microwave Theory and Techniques*, vol. 65, no. 5, pp. 1780-1794, 2017.

- [5] J. A. Nanzer, *Microwave and Millimeter-wave Remote Sensing for Security Applications*. Artech House, 2012.
- [6] N. A. Salmon *et al.*, "First video rate imagery from a 32-channel 22-GHz aperture synthesis passive millimetre wave imager," in *Millimetre Wave and Terahertz Sensors and Technology IV*, 2011, vol. 8188, p. 818805: International Society for Optics and Photonics.
- [7] D. M. Sheen, D. L. McMakin, and T. E. Hall, "Three-dimensional millimeter-wave imaging for concealed weapon detection," *IEEE Transactions on Microwave Theory and Techniques*, vol. 49, no. 9, pp. 1581-1592, 2001.
- [8] A. Moreira, P. Prats-Iraola, M. Younis, G. Krieger, I. Hajnsek, and K. P. Papathanassiou, "A tutorial on synthetic aperture radar," *IEEE Geoscience and Remote Sensing Magazine*, vol. 1, no. 1, pp. 6-43, 2013.
- [9] R. C. Hansen, *Phased Array Antennas*. Wiley, 2009.
- [10] M. F. Imani *et al.*, "Review of Metasurface Antennas for Computational Microwave Imaging," in *IEEE Transactions on Antennas and Propagation*, vol. 68, no. 3, pp. 1860-1875, March 2020.
- [11] J. A. M. Lorenzo, J. H. Juesas, and W. Blackwell, "A Single-Transceiver Compressive Reflector Antenna for High-Sensing-Capacity Imaging," *IEEE Antennas and Wireless Propagation Letters*, vol. 15, pp. 968-971, 2016.
- [12] L. Yujiri, M. Shoucri and P. Moffa, "Passive millimeter wave imaging," in *IEEE Microwave Magazine*, vol. 4, no. 3, pp. 39-50, Sept. 2003.
- [13] M. Shoucri *et al.*, "A passive millimeter wave camera for aircraft landing in low visibility conditions," in *IEEE Aerospace and Electronic Systems Magazine*, vol. 10, no. 5, pp. 37-42, May 1995.
- [14] A. R. Thompson, J. M. Moran, and G. W. Swenson, *Interferometry and Synthesis in Radio Astronomy*. Wiley, 2001.
- [15] C. S. Ruf, C. T. Swift, A. B. Tanner and D. M. Le Vine, "Interferometric synthetic aperture microwave radiometry for the remote sensing of the Earth," in *IEEE Transactions on Geoscience and Remote Sensing*, vol. 26, no. 5, pp. 597-611, Sept. 1988.

- [16] M. Born and E. Wolf, Principles of Optics. Cambridge, U.K.:Cambridge Univ. Press, 1999
- [17] S. Vakalis and J. A. Nanzer, "Microwave imaging using noise signals," *IEEE Transactions on Microwave Theory and Techniques*, vol. 66, no. 12, pp. 5842-5851, 2018.
- [18] S. Vakalis and J. A. Nanzer, "Analysis of Array Sparsity in Active Incoherent Microwave Imaging," *IEEE Geoscience and Remote Sensing Letters*, pp. 1-5, 2019.
- [19] R. M. Narayanan and M. Dawood, "Doppler estimation using a coherent ultrawide-band random noise radar," in *IEEE Transactions on Antennas and Propagation*, vol. 48, no. 6, pp. 868-878, June 2000.
- [20] S. Holm, A. Austeng, K. Iranpour, and J.-F. Hopperstad, "Sparse Sampling in Array Processing," in *Nonuniform Sampling: Theory and Practice*, F. Marvasti, Ed. Boston, MA: Springer US, 2001, pp. 787-833.
- [21] J. A. Nanzer, "Millimeter-wave interferometric imaging sensors," in *SENSORS*, 2013 IEEE, 2013, pp. 1-4.
- [22] A. C. Bovik, "Basic tools for image Fourier analysis," in *The Essential Guide to Image Processing*, Academic Press, San Diego, CA, USA, 2009.
- [23] A. Moffet, "Minimum-redundancy linear arrays," in *IEEE Transactions on Antennas and Propagation*, vol. 16, no. 2, pp. 172-175, March 1968.
- [24] H. Nohmi, S. Ohnishi, and O. Kujubu, *Passive millimeter-wave camera with interferometric processing* (Defense and Security Symposium). SPIE, 2006.
- [25] C. Zheng, X. Yao, A. Hu, and J. Miao, "A passive millimeter-wave imager used for concealed weapon detection," Prog. Electromagn. Res. B, vol. 46, pp. 379–397, 2013
- [26] H. Wang, R. M. Narayanan and Z. O. Zhou, "Through-Wall Imaging of Moving Targets Using UWB Random Noise Radar," in *IEEE Antennas and Wireless Propagation Letters*, vol. 8, pp. 802-805, 2009.
- [27] S. Vakalis, L. Gong and J. A. Nanzer, "Imaging With WiFi," in *IEEE Access*, vol. 7, pp. 28616-28624, 2019.
- [28] J. A. Nanzer and R. L. Rogers, "A Ka-band Correlation Radiometer for Human Presence Detection from a Moving Platform," 2007

- *IEEE/MTT-S International Microwave Symposium*, Honolulu, HI, 2007, pp. 385-388.
- [29] S. Vakalis, L. Gong, J. Papapolymerou, and J. A. Nanzer, "40-GHz active interferometric imaging with noise transmitters," *European Radar Conference (EuRAD) October* 2019.
- [30] K. Ahi, "Mathematical Modeling of THz Point Spread Function and Simulation of THz Imaging Systems," in *IEEE Transactions on Terahertz Science and Technology*, vol. 7, no. 6, pp. 747-754, Nov. 2017.
- [31] K. Khare, Fourier Optics and Computational Imaging, Hoboken, NJ, USA:Wiley, pp. 198, 2016.
- [32] D. Kundur and D. Hatzinakos, "Blind image deconvolution," *IEEE Signal Processing Magazine*, vol. 13, no. 3, pp. 43-64, May 1996.

Biographies



Jeffrey A. Nanzer (S'02--M'08--SM'14) received the B.S. degrees in electrical engineering and in computer engineering from Michigan State University, East Lansing, MI, USA, in 2003, and the M.S. and Ph.D. degrees in electrical engineering from The University of Texas at Austin, Austin, TX, USA, in 2005 and 2008, respectively. From

2008 to 2009, he was a Post-Doctoral Fellow with Applied Research Laboratories, University of Texas at Austin, where he was involved in designing electrically small HF antennas and communication systems. From 2009 to 2016, he was with The Johns Hopkins University Applied Physics Laboratory, Laurel, MD, USA, where he created and led the Advanced Microwave and Millimeter-Wave Technology Section. In 2016, he joined the Department of Electrical and Computer Engineering, Michigan State University, where he is currently a Dennis P. Nyquist Assistant Professor. He has authored or coauthored more than 100 refereed journal and conference

papers, authored Microwave and Millimeter-Wave Remote Sensing for Security Applications (Artech House, 2012), and co-authored the chapter "Photonics-Enabled Millimeter-Wave Wireless Systems" in Wireless Transceiver Circuits (Taylor & Francis, 2015). His current research interests include distributed arrays, radar and remote sensing, antennas, electromagnetics, and microwave photonics.

Dr. Nanzer is a member of the IEEE Antennas and Propagation Society Education Committee and the USNC/URSI Commission B. He was a founding member and the First Treasurer of the IEEE APS/MTT-S Central Texas Chapter. He served as the Vice Chair for the IEEE Antenna Standards Committee from 2013 to 2015. He was the Chair of the Microwave Systems Technical Committee (MTT-16), IEEE Microwave Theory and Techniques Society from 2016 to 2018. He was a recipient of the Outstanding Young Engineer Award from the IEEE Microwave Theory and Techniques Society in 2019, the DARPA Director's Fellowship in 2019, the National Science Foundation (NSF) CAREER Award in 2018, the DARPA Young Faculty Award in 2017, and the JHU/APL Outstanding Professional Book Award in 2012. He is currently an Associate Editor of the IEEE TRANSACTIONS ON ANTENNAS AND PROPAGATION.



Stavros Vakalis (S'18)received the Diploma degree in electrical and computer engineering from National Technical University Athens, Athens, Greece in 2017. He is currently pursuing the Ph.D. degree in electrical engineering Michigan State University,

East Lansing, MI, USA. His current research interests include wireless microwave and millimeter-wave systems, millimeter-wave imaging, antenna arrays, radar and signal processing.

Mr. Vakalis has received for his graduate studies the Gerondelis Foundation Graduate Scholarship. He is a member of the IEEE Microwave Theory and Techniques Society and the IEEE Antennas and Propagation Society.

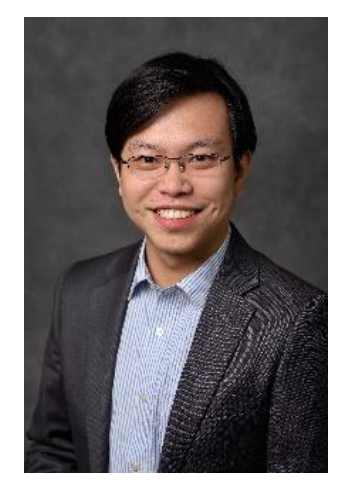
He is currently serving as a reviewer for the IEEE Transactions on Microwave Theory and Techniques, the IEEE Journal of Electromagnetics, RF and Microwaves in Medicine and Biology, and the IEEE Transactions on Antennas and Propagation.



Liang Gong received his B.Eng. degree in Electrical Engineering from the Xidian University, Xi'an, China in 2008. In 2012, he joined the Microsystems Research Group in the School of Electrical Engineering and

Telecommunications, University of New South Wales (UNSW), Sydney, Australia, where he got the M.EngSc. degree in 2013

and the Ph.D. degree in 2017. From 2018 to 2019, he was a postdoctoral research associate at the Department of Electrical and Computer Engineering, Michigan State University (MSU), jointly with UNSW. His research interests include the RF MEMS, antennas, millimeterwave circuits and systems, radar and interferometric imaging systems. He is currently an antenna engineer in Amazon (Kuiper Project).



Yuxiao He received his B.S. degree in Communications Engineering from Communication University of China, Beijing, China in 2013, and M.S degree in Electrical Engineering from University at Buffalo, the State University of New York, Buffalo, NY, USA in 2016, and Ph.D degree in Electrical Engineering in Michigan State University, East Lansing, MI, USA in

2020. He is currently a RF R&D engineer in Starry Inc., Boston, USA. His research interests include microwave

and millimeter-wave circuits and components, reconfigurable RF devices, RF applications of nanomagnetic thin films and additive manufacturing.



John Papapolymerou (F'11) received the B.S.E.E. degree from the National Technical University of Athens, Athens, Greece, in 1993, the M.S.E.E. and Ph.D. degrees from the University of Michigan, Ann Arbor, in 1994 and 1999, respectively. From 1999-2001 he was an Assistant Professor at the Department of Electrical

and Computer Engineering of the University of Arizona, Tucson and during the summers of 2000 and 2003 he was a visiting professor at The University of Limoges, France. From 2001-2005, 2005-2009 and 2009-2013 he was an Assistant Professor, Associate Professor and Professor, respectively, at the School of Electrical and Computer Engineering (ECE) of the Georgia Institute of Technology. From 2013-2015 he was the Ken Byers Professor at the School of ECE at Georgia Tech; he was also the Associate Director of the Georgia Electronic Design Center (GEDC) from 2011-2015. As of August 2015 he is the MSU Foundation Professor and Chair of the Electrical and Computer Engineering Department at Michigan State University. He was selected as an MSU Academic Leadership Program (ALP) Fellow of the Big-Ten Academic Alliance during the 2018-19 academic year. He has graduated 27 PhD students and has advised more than 50 post-doctoral fellows, graduate and undergraduate students throughout his career. He has authored or coauthored over 400 publications in peerreviewed journals and conferences and holds 5 US patents. His research interests include the implementation of additive manufacturing technologies in microwave, millimeter-wave and THz circuits and the development of both passive and active planar circuits and antennas on semiconductor (Si/SiGe, GaAs), organic (liquid crystal polymer-LCP) and 3-D printed substrates for System-ona-Chip (SOC)/ System-on-a-Package (SOP) RF front ends.

Dr. Papapolymerou served as General Co-Chair of the 2019 IEEE International Symposium on Antennas and Propagation, and as Editor-in-Chief for IEEE Microwave and Wireless Components Letters (MWCL) from 2012-2015. He has also served as an Associate Editor for IEEE Transactions on Microwave Theory and Techniques from 2010-2012, and as Chair for Commission D of the US National Committee of URSI from 2009-2011. He was also Associate Editor for IEEE MWCL (2004-2007), and IEEE Transactions on Antennas and Propagation (2004-2010). During 2004, he was the Chair of the IEEE MTT/AP Atlanta Chapter. He was the recipient of the 2012 IEEE Antennas and Propagation Society (AP-S) H.A. Wheeler Prize Paper Award, the 2010 IEEE AP-S John Kraus Antenna Award, the 2009 IEEE Microwave Theory and Techniques-Society (MTT-S) Outstanding Young Engineer Award, the 2009 Georgia Tech School of ECE Outstanding Junior Faculty Award, the 2004 Army Research Office (ARO) Young Investigator Award, the 2002 National Science Foundation (NSF) CAREER award, the best paper award at the 3rd IEEE International Conference on Microwave and Millimeter-Wave Technology (ICMMT2002), Beijing, China and the 1997 Outstanding Graduate Student Instructional Assistant Award presented by the American Society for Engineering Education (ASEE), The University of Michigan Chapter.